J. Fluid Mech. (1969), *vol.* 35, *part* 2, *pp.* 369–386
Printed in Great Britain

Numerical solution for the flow around a cylinder at Reynolds numbers of 40, 200 and 500

By JAIME S. SON† AND THOMAS J. HANRATTY

Department of Chemistry and Chemical Engineering, University of Illinois, Urbana, Illinois

(Received 22 July 1968)

Finite difference solutions for the time dependent equations of motion have been carried out in order to extend the range of available data on steady flow around a cylinder to larger Reynolds numbers. At the termination of the calculations for $R = 40$ and 200, the separation angle, the drag coefficient and the pressure and vorticity distributions around the surface of the cylinder were very close to their steady-state values. For $R = 500$ the separation angle and drag coefficient were very close to their steady-state values but the pressure distribution and vorticity distribution at the rear of the cylinder were still changing slightly. The results at $R = 500$ were found to be quite different from those at $R = 200$ so it is not clear how closely we approximated the steady solution for $R \to \infty$. The forces on the cylinder due to viscous drag and due to pressure drag are found to be smaller for steady flow than for laboratory experiments where the wake is unsteady.

1. Introduction

Although a large number of numerical calculations of the flow around a cylinder have been presented in the literature, no reliable steady flow solutions have been obtained for Reynolds numbers greater than 50. This paper reports on some of the results of finite difference calculations of the time dependent equations of motion at $R = 40$, $R = 200$ and $R = 500$ for the case of a fluid of infinite extent. The outer boundary, r_∞, used for the calculations was large enough that at the termination of the calculation the wake from the cylinder had not yet been convected to r_∞. Actually the flow field never becomes steady since the wake continues to grow. The goal was to terminate the calculations at sufficiently large times that the velocity field near the wall, the pressure field at the wall, and, hopefully, the length of the wake bubble had closely approached the values they would assume at infinite time. The papers by Pearson (1965) and by Wilkes & Churchill (1966) have been particularly useful for these calculations.

The first successful numerical solution of the complete equations of motion in two dimensions was obtained by Thom (1928) for flow around a circular cylinder at Reynolds number, $R = 10$. Later Thom (1933) improved his numerical method by a transformation of the physical plane and obtained a solution at $R = 20$ which agrees with available experimental results. Kawaguti (1953*b*) and Apelt

† Present address: Shell Development Company, Emeryville, California.

(1961) used slightly modified versions of Thom's method to carry out calculations at $R = 40$. Allen & Southwell (1955) used a relaxation technique to obtain solutions for $R = 0$, 1, 10, 100 and 10,000. Dennis & Shimshoni (1965) reduced the equations of motion to a series of ordinary differential equations and solved these by a numerical method over the range of R from 0·01 to 10^5. Allen & Southwell found that the length of the vortices behind the cylinder starts to decrease between $R = 10$ and $R = 100$ and Dennis & Shimshoni found a decrease after $R = 30$. Since these results seem to be in disagreement with experiment the accuracy of their calculations at high Reynolds numbers has been questioned.

The numerical solutions discussed above have been obtained using the equations of motion for a steady flow. Payne (1958) carried out a numerical integration of the time dependent equations of motion at $R = 40$ and at $R = 100$ but did not proceed far enough to reach steady state. Kawaguti & Jain (1966) reported numerical solutions of the time dependent equations for $R = 10$, 20, 30, 40, 50, 60 and 100. Steady state was reached for $R = 10$, 20, 30, 40 and 50.

Thoman & Szewczyk (1966) solved the time dependent equations for $R = 1$ to $R = 1 \times 10^6$. Steady flow solutions were obtained at large times for $R = 1$ and for $R = 30$. At larger Reynolds numbers antisymmetric disturbances were introduced after the solutions had been carried out to a certain dimensionless time. The disturbances caused alternate shedding of the vortices behind the cylinder and the formation of a vortex street.

The motivation behind the research described in this paper was to obtain some insight into the nature of the steady flow field at infinite Reynolds number. Since an analytical solution of the Navier–Stokes equations is not available a number of models have been suggested which could provide a basis for calculating the flow field. Confirmation is lacking since laboratory studies at high Reynolds numbers usually involve unsteady flows.

The model of Kelvin and Helmholtz (Kawaguti 1953*a*; Squire 1934) assumes that the wake is enclosed by two free-streamlines which are idealized shear layers. The fluid inside the wake is assumed to have zero velocity and to be at the same pressure as the free stream. Batchelor (1956) suggested that the wake is closed, finite and of uniform vorticity. Acrivos, Snowden, Grove & Peterson (1965) were able to obtain steady flows up to a Reynolds number of 180 by placing a splitter plate in the wake of the cylinder. On the basis of these experiments they suggested that at infinite Reynolds number the wake bubble is viscous, that it has an infinite length and a width of the order of magnitude of the cylinder diameter, and that the pressure coefficient at the rear stagnation point is approximately equal to $-0{\cdot}45$.

Unfortunately we were not completely successful in attaining our original goals. The flow at $R = 500$ is found to be significantly different from the flow at $R = 200$ so it is not clear how closely the results approached the asymptotic behaviour for $R \to \infty$.

2. Numerical procedures

The equations describing the variation of the vorticity, ζ, and the stream function, ψ, are

$$r\frac{\partial\zeta}{\partial t}+\frac{\partial\psi}{\partial\theta}\frac{\partial\zeta}{\partial r}-\frac{\partial\psi}{\partial r}\frac{\partial\zeta}{\partial\theta}=\frac{2}{R}\left[r\frac{\partial^2\zeta}{\partial r^2}+\frac{\partial\zeta}{\partial r}+\frac{1}{r}\frac{\partial^2\zeta}{\partial\theta^2}\right], \tag{1}$$

$$\zeta=\frac{1}{r}\left[\frac{\partial}{\partial r}\left(r\frac{\partial\psi}{\partial r}\right)+\frac{1}{r}\frac{\partial^2\psi}{\partial\theta^2}\right], \tag{2}$$

where the terms have been normalized using the radius of the cylinder, a, and the velocity of the fluid at infinity, U_∞. The Reynolds number is defined as $R=2aU_\infty/\nu$. The angle θ is measured from the rear of the cylinder. The boundary conditions are

$$\psi=\partial\psi/\partial r=0 \quad \text{for} \quad r=1, \tag{3}$$

$$\zeta\to 0, \quad \psi\to r\sin\theta \quad \text{for} \quad r\to\infty, \tag{4}$$

$$\psi=\zeta=0 \quad \text{for} \quad \theta=0,\pi. \tag{5}$$

Since it is desirable to have a finer mesh near the cylinder surface the following transformation of the independent variables has been made

$$r=e^{\pi\xi}, \quad \eta=\theta/\pi. \tag{6}$$

The defining equations then become

$$E^2\frac{\partial\zeta}{\partial\tau}+\frac{\partial\psi}{\partial\eta}\frac{\partial\zeta}{\partial\xi}-\frac{\partial\psi}{\partial\xi}\frac{\partial\zeta}{\partial\eta}=\frac{2}{R}\left[\frac{\partial^2\zeta}{\partial\eta^2}+\frac{\partial^2\zeta}{\partial\xi^2}\right], \tag{7}$$

$$E^2\zeta=\frac{\partial^2\psi}{\partial\eta^2}+\frac{\partial^2\psi}{\partial\xi^2}, \tag{8}$$

$$\psi=\frac{\partial\psi}{\partial\xi}=0 \quad \text{for} \quad \xi=1, \tag{9}$$

$$\zeta\to 0, \quad \psi\to e^{\pi\xi}\sin\pi\eta \quad \text{as} \quad \xi\to\infty, \tag{10}$$

$$\psi=\zeta=0 \quad \text{for} \quad \eta=0,1, \tag{11}$$

$$E=\pi e^{\pi\xi}. \tag{12}$$

Figure 1 shows a portion of the network of grid points. Let n denote the number of time steps and $\Delta\tau$, the size of the time step. The scheme for advancing the solution from time $n\Delta\tau$ to time $(n+1)\Delta\tau$ consists of calculating new values of the vorticity, $\zeta_{i,j}^{n+1}$, at all grid points from the finite-difference approximation of (7), the boundary conditions and the values of the vorticity, $\zeta_{i,j}^{n}$, and the stream function, $\psi_{i,j}^{n}$, from the previous time step. New values of the stream function $\psi_{i,j}^{n+1}$ are calculated for all grid points by using the finite-difference approximation of (8), the boundary conditions, the new values of the vorticity $\zeta_{i,j}^{n+1}$, and the old values of the stream function $\psi_{i,j}^{n}$.

An alternating-direction-implicit method developed by Peaceman & Rachford (1955) is used to calculate values of the vorticity at the new time step. The

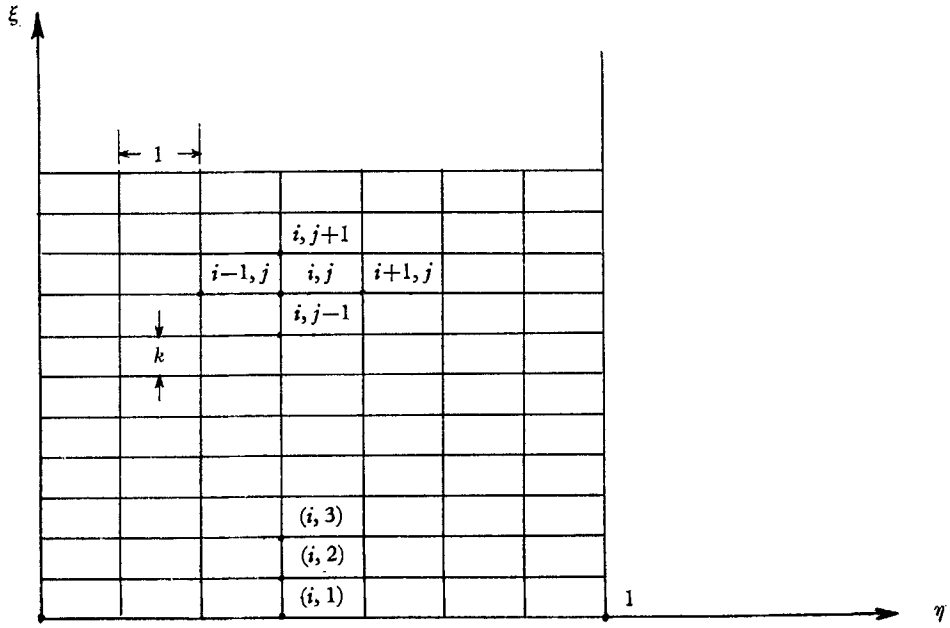

FIGURE 1. The grid structure.

method divides the time step, $\Delta\tau$, into two half-steps, $\frac{1}{2}\Delta\tau$, and the following two finite-difference approximations are obtained:

$$\frac{E^2}{\frac{1}{2}\Delta\tau}(\zeta_{i,j}^{n+\frac{1}{2}}-\zeta_{i,j}^{n})+\left[\frac{1}{2l}(\psi_{i+1,j}^{n}-\psi_{i-1,j}^{n})\right]\left[\frac{1}{2k}(\zeta_{i,j+1}^{n}-\zeta_{i,j-1}^{n})\right]$$
$$-\left[\frac{1}{2k}(\psi_{i,j+1}^{n}-\psi_{i,j-1}^{n})\right]\left[\frac{1}{2l}(\zeta_{i+1,j}^{n+\frac{1}{2}}-\zeta_{i-1,j}^{n+\frac{1}{2}})\right]$$
$$=\frac{2}{R}\left[\frac{1}{l^2}(\zeta_{i+1,j}^{n+\frac{1}{2}}-2\zeta_{i,j}^{n+\frac{1}{2}}+\zeta_{i-1,j}^{n+\frac{1}{2}})+\frac{1}{k^2}(\zeta_{i,j+1}^{n}-2\zeta_{i,j}^{n}+\zeta_{i,j-1}^{n})\right], \tag{13}$$

$$\frac{E^2}{\frac{1}{2}\Delta\tau}(\zeta_{i,j}^{n+1}-\zeta_{i,j}^{n+\frac{1}{2}})+\left[\frac{1}{2l}(\psi_{i+1,j}^{n}-\psi_{i-1,j}^{n})\right]\left[\frac{1}{2k}(\zeta_{i,j+1}^{n+1}-\zeta_{i,j-1}^{n+1})\right]$$
$$-\left[\frac{1}{2k}(\psi_{i,j+1}^{n}-\psi_{i,j-1}^{n})\right]\left[\frac{1}{2l}(\zeta_{i+1,j}^{n+\frac{1}{2}}-\zeta_{i-1,j}^{n+\frac{1}{2}})\right]$$
$$=\frac{2}{R}\left[\frac{1}{l^2}(\zeta_{i+1,j}^{n+\frac{1}{2}}-2\zeta_{i,j}^{n+\frac{1}{2}}+\zeta_{i-1,j}^{n+\frac{1}{2}})+\frac{1}{k^2}(\zeta_{i,j+1}^{n+1}-2\zeta_{i,j}^{n+1}+\zeta_{i,j-1}^{n+1})\right]. \tag{14}$$

Equations (13) and (14) are implicit in the η- and ξ-directions. Their solutions are obtained by the method of Thomas (Lapidus 1962).

The solution of the stream function equation is obtained by the extrapolated-Liebmann method (Fox 1962; Lapidus 1962). The finite difference approximation

to (8) is

$$\psi_{i,j}^{m+1} = (1-\alpha)\,\psi_{i,j}^{m} + \frac{\alpha}{2\left(\frac{1}{l_2}+\frac{1}{k^2}\right)} \times\left[\frac{1}{l^2}(\psi_{i+1,j}^{m}+\psi_{i-1,j}^{m+1})+\frac{1}{k^2}(\psi_{i,j+1}^{m}+\psi_{i,j-1}^{m+1})-E^2\zeta_{i,j}^{n+1}\right], \quad (15)$$

where $\psi_{i,j}^{m}$ and $\psi_{i,j}^{m+1}$ are the approximations to the stream function at the mth and $(m+1)$th iteration and α is the relaxation factor. The equation proposed by Russel (1962),

$$\alpha_0 = \frac{2}{1+\pi[(I^{-2}+J^{-2})/2]^{\frac{1}{2}}}, \quad (16)$$

has been found to give a good value of α. The quantities I and J are respectively the number of meshes in η- and ξ-directions. The extrapolated-Liebmann method consists of applying (15) at every internal mesh point in regular succession. The points are scanned row by row from left to right starting from the row next to the boundary and going up the paper (see figure 1). This completes one iteration. The procedure is repeated until values of the stream function in two successive iterations satisfy the equation

$$|\psi_{i,j}^{m+1}-\psi_{i,j}^{m}| \leqslant 10^{-6} \quad (17)$$

at all interior grid points.

The vorticity distribution around the surface of the cylinder must be known in order to carry out the finite difference calculations. It is obtained from the values of ψ near the wall. The Taylor series expansions for the stream function at points given by the co-ordinates $(i, 2)$ and $(i, 3)$ shown in figure (1) are

$$\psi_{i,2} = \psi_{i,1} + k\left(\frac{\partial\psi}{\partial\xi}\right)_{i,1} + \frac{k^2}{2}\left(\frac{\partial^2\psi}{\partial\xi^2}\right)_{i,1} + \ldots, \quad (18)$$

$$\psi_{i,3} = \psi_{i,1} + 2k\left(\frac{\partial\psi}{\partial\xi}\right)_{i,1} + \frac{(2k)^2}{2}\left(\frac{\partial^2\psi}{\partial\xi^2}\right)_{i,1} + \ldots. \quad (19)$$

These two equations, together with (8) and the boundary conditions

$$\psi_{i,1} = \left(\frac{\partial\psi}{\partial\xi}\right)_{i,1} = 0 \quad \text{and} \quad \left(\frac{\partial^2\psi}{\partial\eta^2}\right)_{i,1} = 0$$

yield the following relation $\zeta_{i,1} = \dfrac{8\psi_{i,2}-\psi_{i,3}}{2E^2k^2}$. (20)

The value of ψ at the outer boundary of the grid ξ_∞ should be given by the following equation as $\xi_\infty \to \infty$

$$\psi_{i,J+1} = e^{\pi\xi_\infty}\sin\pi\eta. \quad (21)$$

The procedure used in this study was to select ξ_∞ large enough so that it is justified to use (21).

The pressure variation around the surface of the cylinder is given as

$$P_{\xi=0} = -\frac{4}{R}\int_0^{\eta}\left(\frac{\partial\zeta}{\partial\xi}\right)_{\xi=0} d\eta + \text{constant}, \quad (22)$$

where the pressure has been normalized with respect to $\frac{1}{2}\rho U_\infty^2$. The contribution

of the pressure forces to the drag coefficient is

$$C_P = \int_0^{\pi} P_{\xi=0} \cos\theta \, d\theta. \tag{23}$$

The frictional contribution to the drag coefficient is calculated as follows

$$C_f = -\frac{4}{R}\int_0^{\pi} \zeta_{\xi=0} \sin\theta \, d\theta. \tag{24}$$

The total drag is defined as $C_D = C_P + C_f.$ (25)

3. Computational procedure

The initial values of ψ are obtained by calculating $\psi_{i,j}$ at every interior grid point by using the potential flow solution,

$$\psi_{i,j} = e^{\pi\xi}\left(\frac{1}{1-e^{\pi\xi}}\right)\sin\pi\eta, \tag{26}$$

and by then applying (15) along with the appropriate boundary conditions until (17) is satisfied. For this computation, the values of $\zeta_{i,j}$ are assumed to be zero. The initial values of the vorticity at the wall are next computed from (20), and $\zeta_{i,j} = 0$ for the rest of the flow field.

Time is stepped by $\Delta\tau$, and new values of the vorticity are computed from (13) and (14). The new values of the stream function are computed by applying (15) repeatedly until (17) is satisfied. The new values of the vorticity at the boundary are calculated using (20). The above procedure is repeated for successive $\Delta\tau$.

The computations were carried out on the University of Illinois IBM 7094 and IBM 360/Model 50/75 computers. The dimensionless time step used in all runs was 0·04 and the solutions were carried out to the dimensionless times shown in table 1. The total computer times for the IBM 360/Model 75 are also given in

R	l	k	r_∞	τ	Number of net points	Computer time (h)
40	$\frac{1}{30}$	0·03	111·3	50	1581	$\frac{2}{3}$
40	$\frac{1}{30}$	0·025	59·4	41·9	1643	$\frac{2}{3}$
200	$\frac{1}{40}$	0·01	152·4	56·1	6601	7
500	$\frac{1}{60}$	0·007	157·3	67·4	14,091	19

TABLE 1. Summary of parameters used in calculations

table 1 along with the parameters l, k and r_∞ used in the calculations. The reciprocal of l represents the number of increments in the θ direction.

The effect of r_∞ was examined only for $R = 40$. A change from 111·3 to 59·4 had only a very slight effect on the results of the calculation.

4. Results

Reynolds number = 40

For $R = 40$, a small eddy was first observed at $\tau = 0{\cdot}7$. The radial distance from the centre of the cylinder to the tip of the eddy, r_w, increased at the rate shown in figure 2. At $\tau = 22$, the eddy attained its full length, $r_w = 6{\cdot}0$. This is in

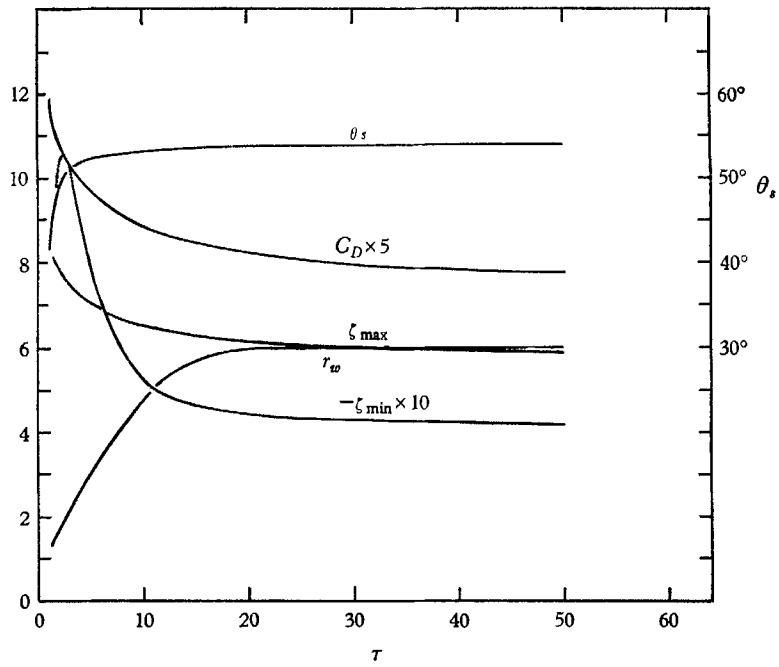

FIGURE 2. The development of ζ_{max}, ζ_{min}, C_D, θ_s and r_w with τ, $R = 40$.

excellent agreement with the value, $r_w = 6{\cdot}03$, obtained by Kawaguti & Jain (1966) at the same Reynolds number for $\tau = 24$. The length is much longer than the $r_w = 4{\cdot}5$ obtained by Kawaguti (1953*b*) and the $r_w = 5{\cdot}27$ obtained by Apelt (1961) by solving the equations of motion for steady state. These differences have been explained by Kawaguti & Jain (1966) as due to the coarseness of the mesh used by Apelt and by Kawaguti in their solutions of steady-state equations. The streamlines at $\tau = 50$ are plotted in figure 3. This plot compares favourably with the photograph of the flow pattern obtained by Taneda (1956) at $R = 42$.

Figure 2 also shows how the separation angle, θ_s, the maximum and minimum values of the vorticity, ζ_{max} and ζ_{min}, and the drag coefficient vary with time. The separation point reaches a steady value of 53·9° as early as $\tau = 28$. This is to be compared with values of 50·0°, 52·5° and 53·7° obtained by Kawaguti (1953*a*, *b*), Apelt (1961) and Kawaguti & Jain (1966). The rate of change of ζ_{max}, ζ_{min} and C_D was rather slow but the values at $\tau = 50$ seem close to steady state. The development of the vorticity distribution and pressure distribution around the surface is shown in figures 4 and 5. The pressure term appearing in the ordinate in figure 5 is relative to the pressure at the rear stagnation point.

Reynolds number = 200

At $R = 200$ the eddy was first observed at $\tau = 0{\cdot}36$. The streamline patterns at an early time, $\tau = 5{\cdot}3$, and at the end of the computation, $\tau = 56{\cdot}1$, are shown in figures 6 and 7. The length of the wake bubble was difficult to determine at large

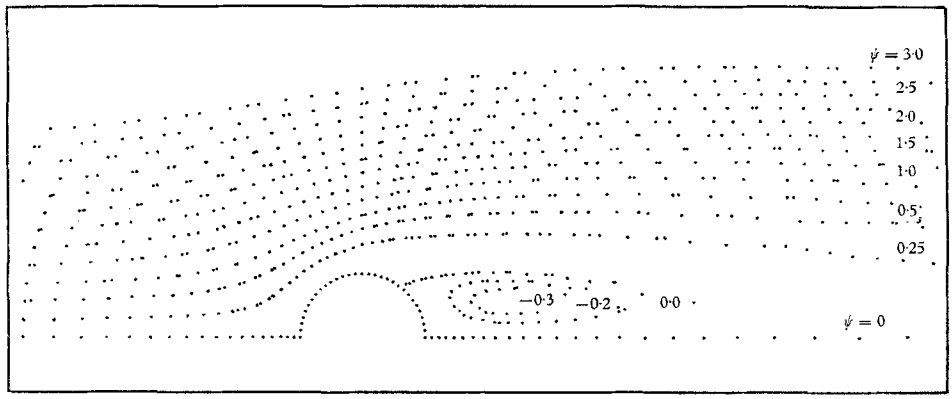

FIGURE 3. Steamlines, $R = 40$, $\tau = 50$.

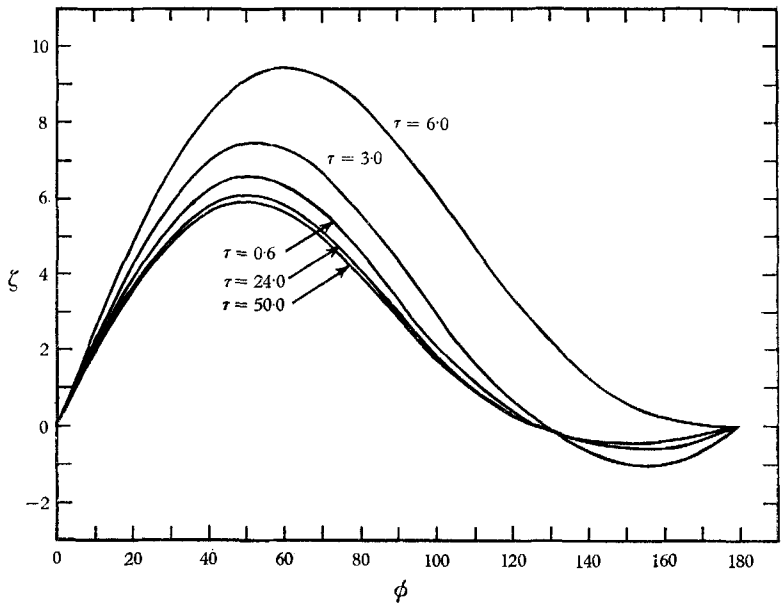

FIGURE 4. The development of surface vorticity distribution, $R = 40$.

times because of the large distances between grid points in the angular direction at large values of r. For this reason the values could be in error. The length r_w is estimated to be 13 at $\tau = 56{\cdot}1$.

Figure 8 shows the change of θ_s, $\zeta_{\max}$, $\zeta_{\min}$, r_w and C_D with time. The separation angle, θ_s, approaches a steady value of 75° at an early time, $\tau = 25$. All of the

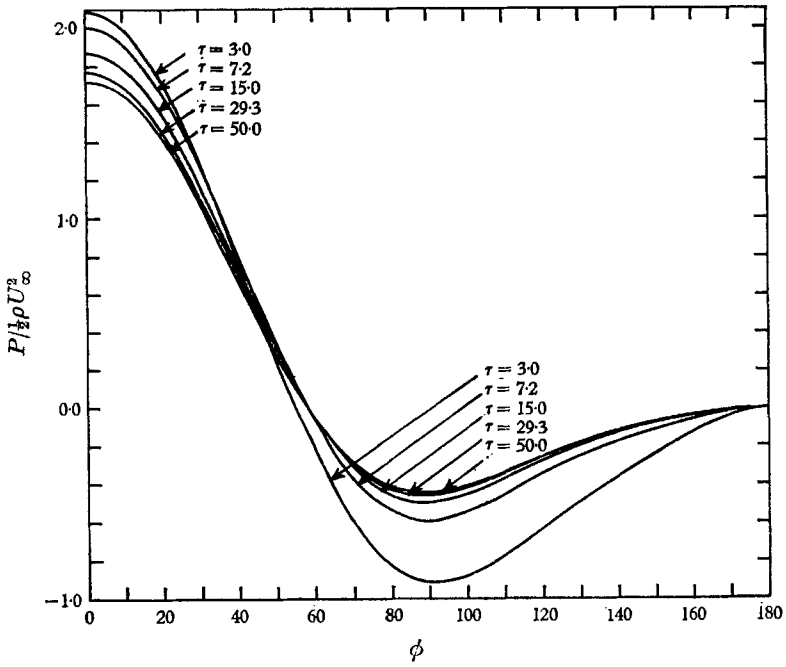

FIGURE 5. The development of surface pressure distribution, $R = 40$.

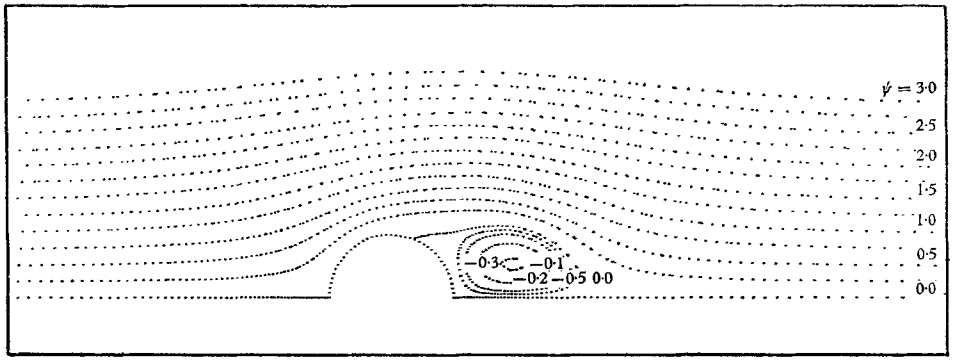

FIGURE 6. Streamlines, $R = 200$, $\tau = 5{\cdot}3$.

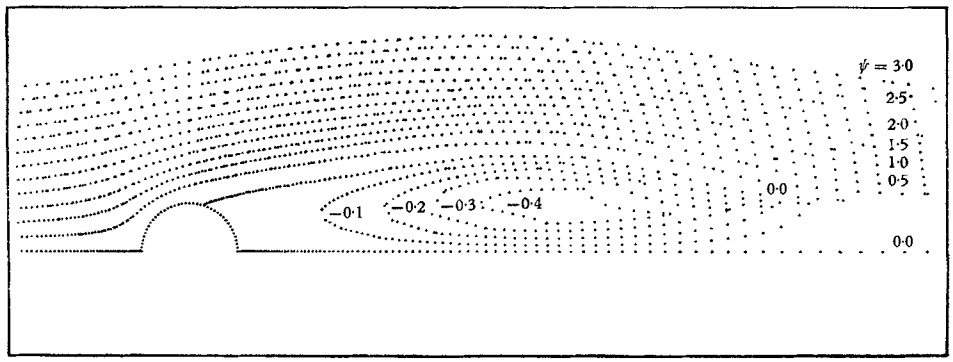

FIGURE 7. Streamlines, $R = 200$, $\tau = 56{\cdot}1$.

other quantities, with exception of r_w, approached steady values at $\tau = 45$. The development of the vorticity distribution and the pressure distribution around the surface is shown in figures 9 and 10. Of particular interest are the two minima in the wall vorticity which eventually appear in the wake and which persist up to steady state.

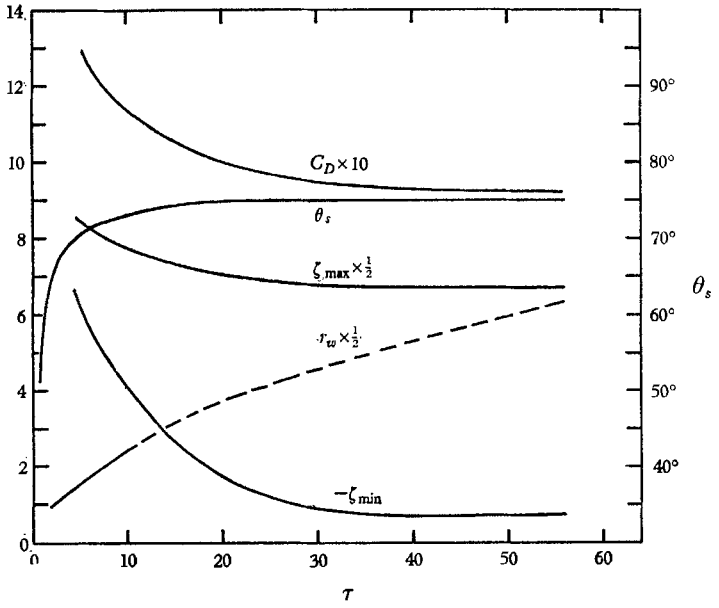

FIGURE 8. The development of ζ_{max}, ζ_{min}, C_D, θ_s and r_w with τ, $R = 200$.

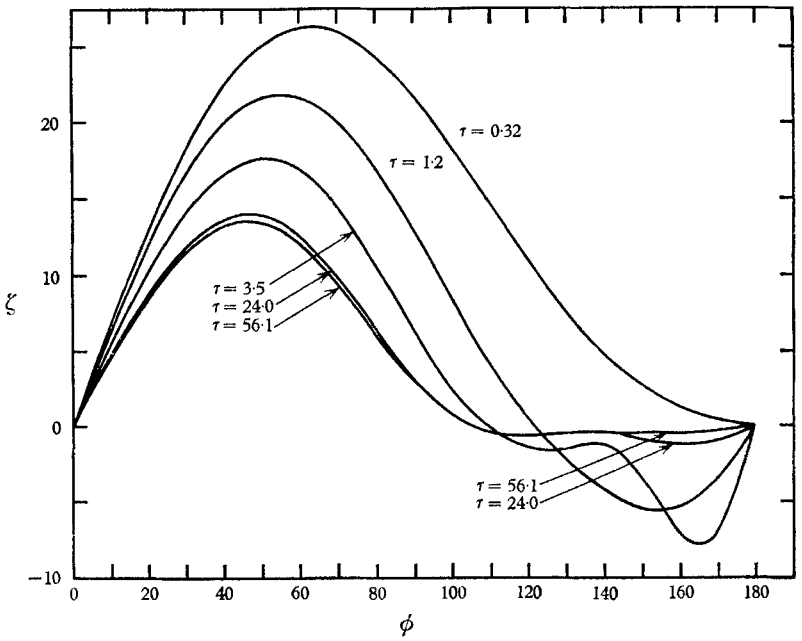

FIGURE 9. The development of surface vorticity distribution, $R = 200$.

Reynolds number = 500

The calculation for $R = 500$ was terminated at $\tau = 67{\cdot}4$. Streamline patterns at $\tau = 8{\cdot}3$ and $\tau = 67{\cdot}4$ for $R = 500$ are shown in figures 11 and 12. As was the case for $R = 200$, the length r_w was difficult to determine at large values of τ. At $\tau = 67{\cdot}4$ it is approximately equal to 10. This is slightly smaller than the value of 13 determined for $R = 200$, $\tau = 56{\cdot}1$.

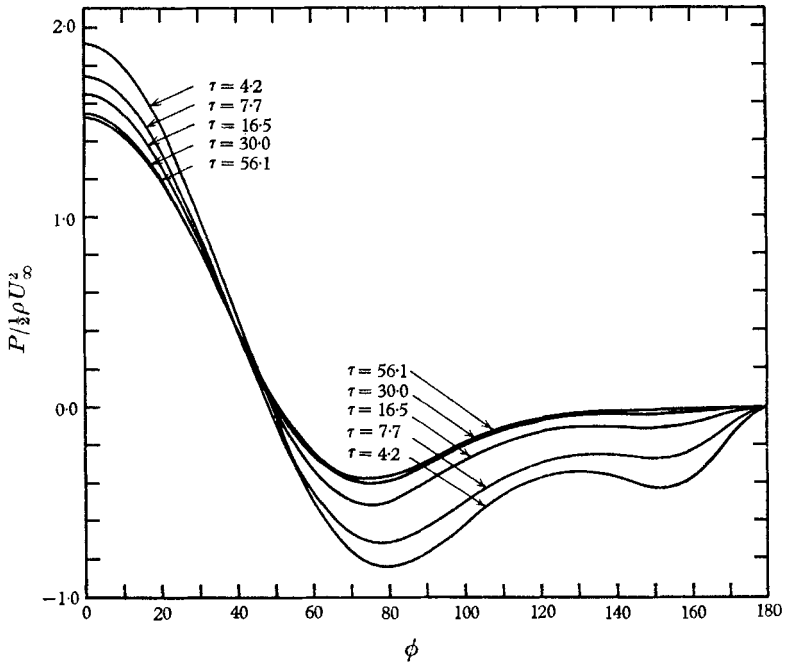

FIGURE 10. The development of surface pressure distribution, $R = 200$.

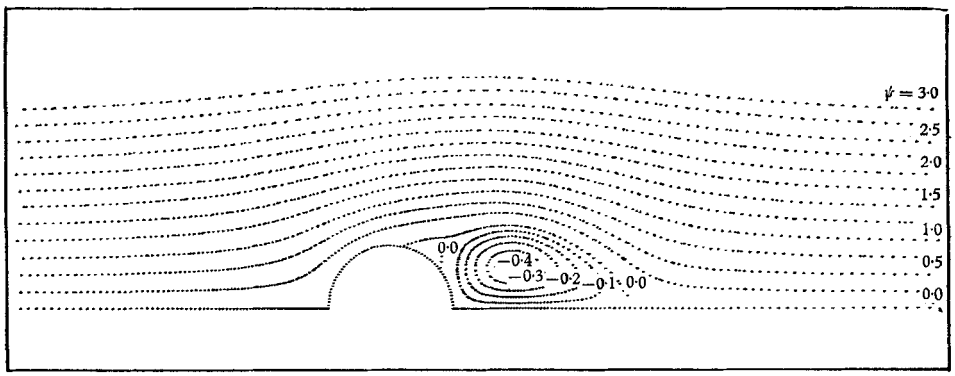

FIGURE 11. Streamlines, $R = 500$, $\tau = 8{\cdot}3$.

Two interesting features about the wake bubble at $R = 500$ are the pronounced fattening of the wake and the appearance near the separation point of a secondary vortex which rotates in the opposite direction of the main vortex. This vortex was first observed at $\tau = 2{\cdot}78$ and can be seen in figure 11 as a line of $\psi = 0$. It

decreased in size after attaining its maximum dimension and disappeared at $\tau \sim 56$. Secondary vortices have also been observed by Thoman & Szewczyk (1966) in their numerical calculations. The calculated streamline patterns for small τ are similar to photographs obtained by Schwabe (1935) of the early vortex formation.

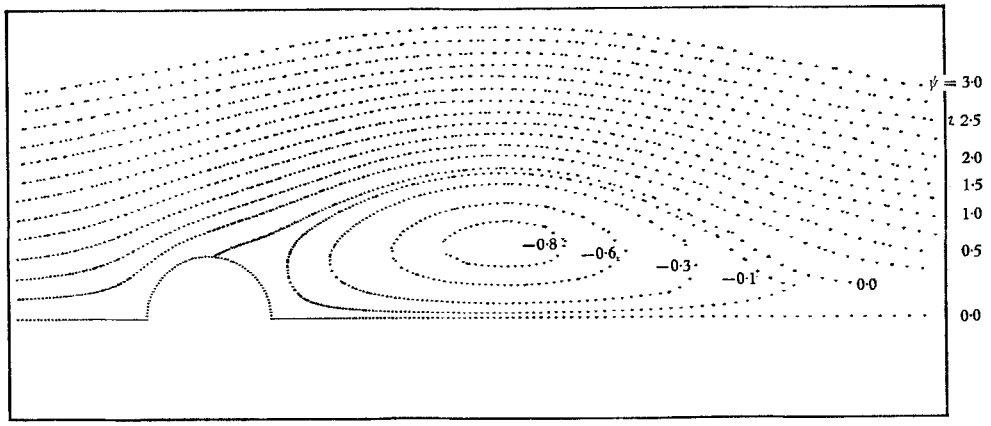

FIGURE 12. Streamlines, $R = 500$, $\tau = 67{\cdot}4$.

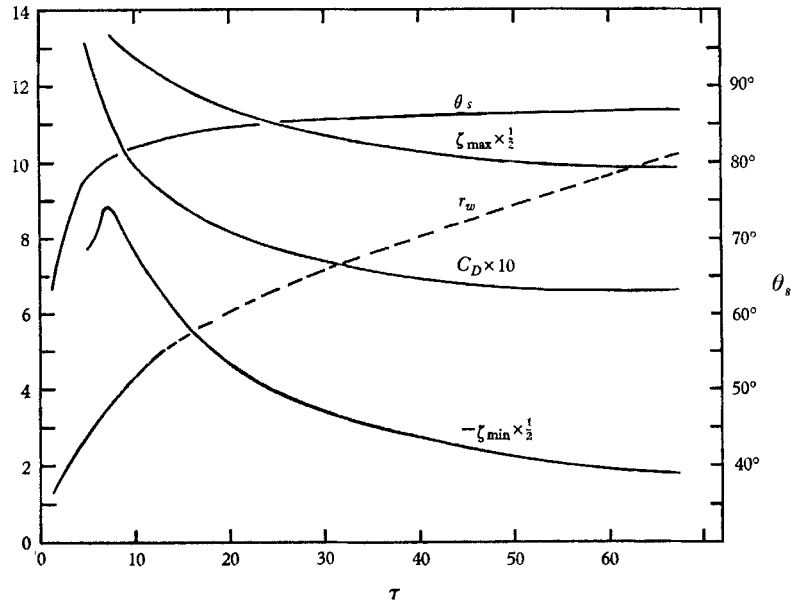

FIGURE 13. The development of ζ_{max}, ζ_{min}, C_D, θ_s and r_w with τ, $R = 500$.

The change of ζ_{max}, ζ_{min}, C_D, θ_s and r_w with time is shown in figure 13. The vorticity distribution and pressure distribution are shown in figures 14 and 15. At the completion of the calculation, $\tau = 67{\cdot}4$, the drag coefficient, C_D, and the separation angle, θ_s, appear very close to their steady-state value. However, the pressure distribution and vorticity distribution appear to be undergoing some

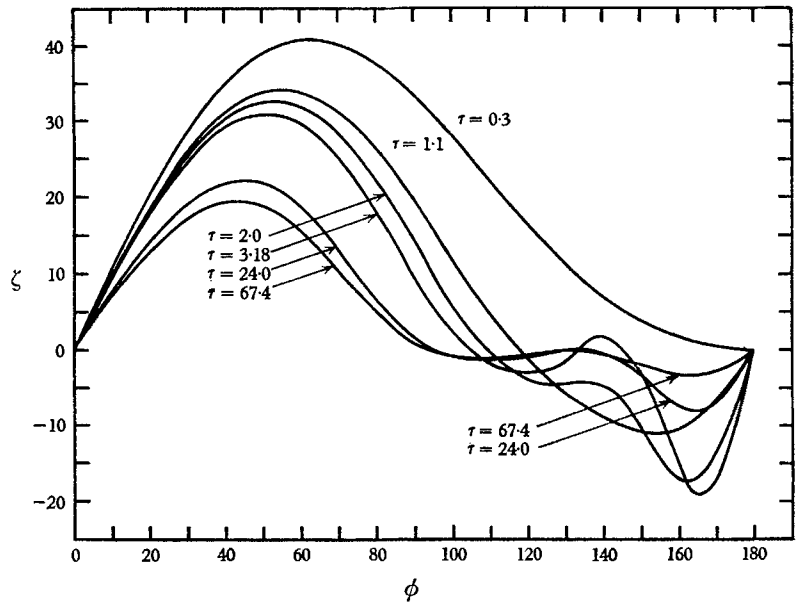

FIGURE 14. The development of surface vorticity distribution, $R = 500$.

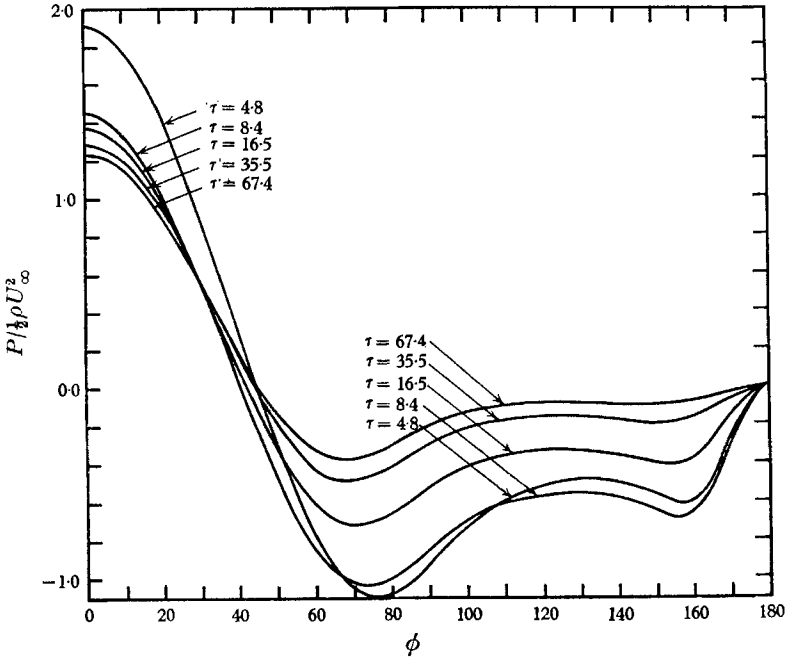

FIGURE 15. The development of surface pressure distribution, $R = 500$.

slight changes. The vorticity distribution at $\tau = 3{\cdot}18$ clearly shows the secondary vortex in the wake as a region of positive vorticity. Again it is of interest to note the two minima in the vorticity that exist in the wake. Pressure distributions obtained by Schwabe (1935) for a cylinder started impulsively from rest at $R = 560$ are similar to those shown in figure 15.

5. Comparison with laboratory experiments

The calculated vorticity distribution at $R = 200$ is compared with measurements by Dimopoulos & Hanratty (1968) in figure 16. The calculations for steady flow are significantly lower than the measurements in the front portion of the cylinder. However, there is some similarity between the calculations and measurements in the rear of the cylinder. The differences are interpreted as being the result of unsteadiness in the experimental wake. The introduction of a splitter plate reduced the difference. However, it appears that the splitter plate did not completely stabilize the wake, even though it did eliminate periodic vortex shedding.

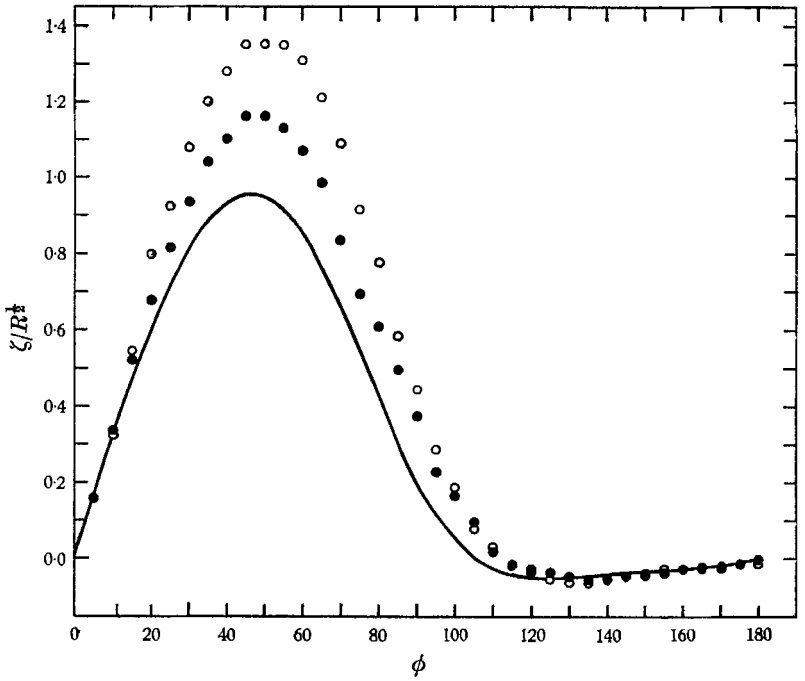

FIGURE 16. Comparison between numerical calculations and measurements (vorticity distribution). Numerical solution: ——, this study, $R = 200$. Experimental measurements: ○, Dimopoulos & Hanratty (1968), $R = 219$, no splitter plate; ●, Dimopoulos & Hanratty (1968), $R = 210$, 4 in. splitter plate.

The effect of the wake on the vorticity distribution is further illustrated in figure 17 where calculations for $R = 40$, $R = 200$ and $R = 500$ are presented. It is seen that in the neighbourhood of the front stagnation point the vorticity is significantly lower than that which would be predicted by boundary layer theory

using the potential solution for the external flow. The difference at $R = 200$ and at $R = 500$ is interpreted as a consequence of the existence of a relatively thick wake. Because of this thick wake the flow approaching the cylinder effectively 'sees' a body of different dimensions than the cylinder.

In figure 18 separation points obtained from numerical calculations are compared with measurements. The agreement is good.

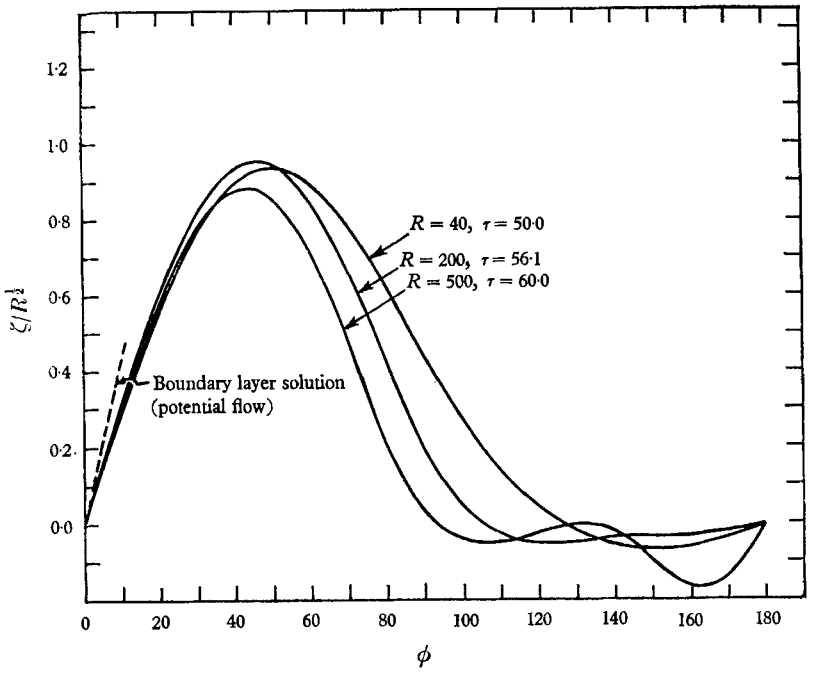

FIGURE 17. Late time vorticity distributions.

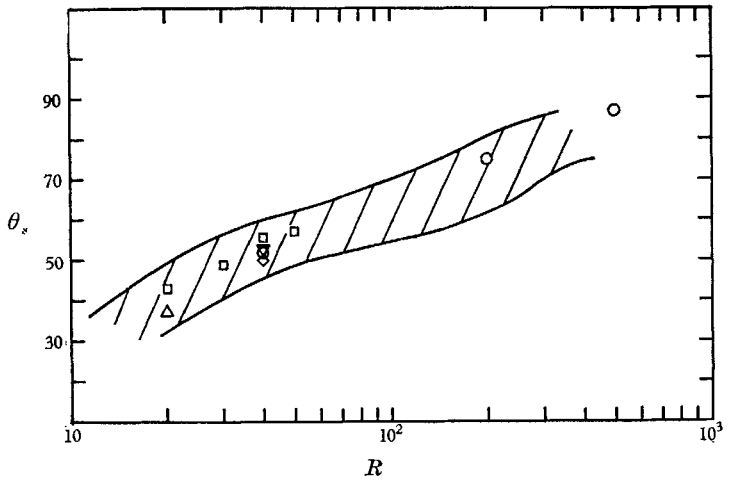

FIGURE 18. Comparison between numerical calculations and measurements (θ_s). Numerical solution: ○, this study; □, Kawaguti & Jain (1966); ◇, Apelt (1961); ▽, Kawaguti (1953*b*); △, Thom (1928). Measurements: shaded area, with and without splitter plate.

Calculated drag coefficients are compared with experimental values in figure 19 and tabulated in table 2. The values for $R = 40$ and $R = 500$ from this study are an extrapolation for $\tau \to \infty$, obtained by plotting C_D versus $1/\tau$. The agreement for $R < 60$ is good. The larger values of C_D observed in the experiments for $R > 60$ are interpreted as due to instabilities in the wake. As can be seen from

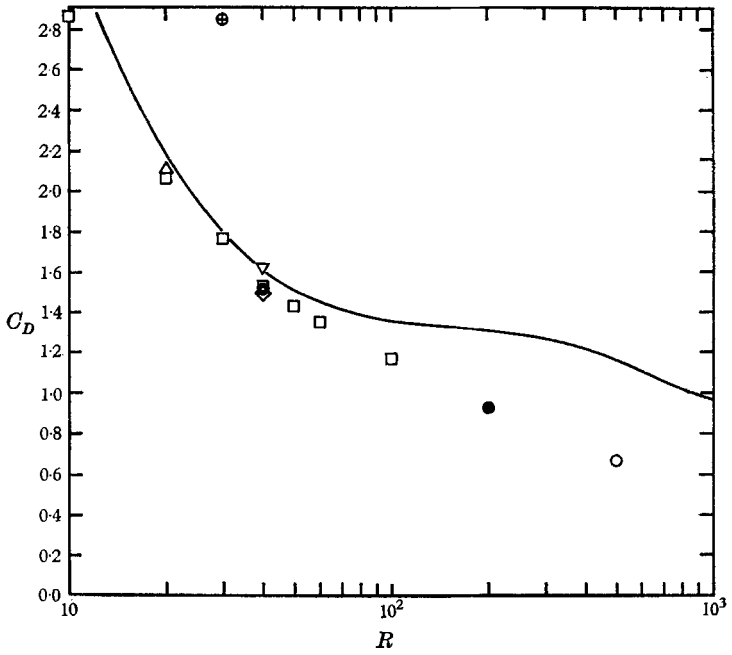

FIGURE 19. Comparison between numerical calculations and measurements (C_D). Numerical solution: ●, this study; ○, this study, extrapolated; □, Kawaguti & Jain (1966), extrapolated; ◇, Apelt (1961); ▽, Kawaguti (1953*b*); △, Thom (1928); ⊕, Thoman & Szewczyk 1966); ——, measurements by Relf.

R	C_D	C_P/C_D
40	1·51	0·660
200	0·924	0·794
500	0·60	0·85

TABLE 2. Calculated drag coefficients for $\tau \to \infty$

the comparison of calculated and experimental vorticity distributions in figure 16 the calculated frictional drag can be expected to be smaller than the experimental. However, this decrease is not large enough to account for the differences shown in figure 19. For example, the numerical solution at $R = 200$ yields a value of $C_f = 0{\cdot}19$, whereas the experimental value of C_f is approximately equal to 0·28. The influence of the wake structure on the form drag, C_P, is the main cause of the smaller drag coefficients obtained for a completely steady wake. A comparison of the pressure distribution measured by Thom (1933) at $R = 174$ with the calcu-

lated one at $R = 200$ is shown in figure 20, where it has been assumed that $(P - P_\infty)/(\frac{1}{2}\rho U_\infty^2)$ at the front stagnation point is the same for the two cases. It is seen that the experimental pressure distribution has a significantly lower minimum.

Support for this research was received from the donors of the Petroleum Research Foundation administered by the American Chemical Society.

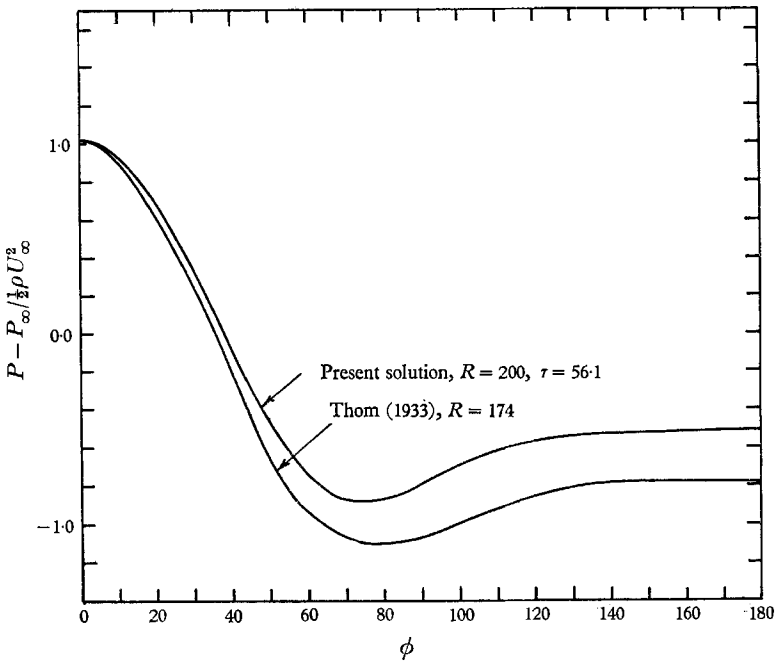

FIGURE 20. Comparison of measured and computed pressure distributions.

REFERENCES

ACRIVOS, A., SNOWDEN, D. D., GROVE, A. S. & PETERSON, E. E. 1965 *J. Fluid Mech.* **21**, 737.

ALLEN, D. N. DE G. & SOUTHWELL, R. V. 1955 *Quart. J. Mech. Appl. Math.* **8**, 129.

APELT, C. J. 1961 *ARC R & M* no. 3175.

BATCHELOR, G. K. 1956 *J. Fluid Mech.* **1**, 388.

DENNIS, S. C. R. & SHIMSHONI, M. 1965 *ARC Current Paper* no. 797.

DIMOPOULOS, H. G. & HANRATTY, T. J. 1968 *J. Fluid Mech.* **33**, 303.

FOX, L., ed. 1962 *Numerical Solutions of Ordinary and Partial Differential Equations.* Massachusetts: Addison-Wesley.

KAWAGUTI, M. 1953*a* *J. Phys. Soc. Japan*, **8**, 403.

KAWAGUTI, M. 1953*b* *J. Phys. Soc. Japan*, **8**, 747.

KAWAGUTI, M. & JAIN, P. 1966 *J. Phys. Soc. Japan*, **21**, 2055.

LAPIDUS, L. 1962 *Digital Computation for Chemical Engineers.* New York: McGraw-Hill.

PAYNE, R. B. 1958 *J. Fluid Mech.* **4**, 81.

PEACEMAN, D. W. & RACHFORD, H. H. 1955 *J. Soc. Indust. Appl. Math.* **3**, 28.

PEARSON, C. 1965 *J. Fluid Mech.* **21**, 611.
RUSSEL, D. B. 1962 *ARC R & M* no. 3331.
SCHWABE, M. 1935 *Ing.-Arch.* **6**, 1; Engl. translation in *NACA Tech. Memo* no. 1039.
SQUIRE, H. B. 1934 *Phil. Mag.* **17**, 1150.
TANEDA, S. 1956 *J. Phys. Soc. Japan*, **11**, 302.
THOM, A. 1928 *ARC R & M* no. 1194.
THOM, A. 1933 *Proc. Roy. Soc.* A **141**, 651.
THOMAN, D. C. & SZEWCZYK, A. A. 1966 *Heat Transfer and Fluid Mech. Lab., Department of Mechanical Engineering, University of Notre Dame. Tech. Rep.* 66-14.
WILKES, J. O. & CHURCHILL, S. W. 1966 *A.I.Ch.E. J.* **12**, 161.